Materials Express

2158-5849/2017/7/043/008
doi:10.1166/mex.2017.1348
www.aspbs.com/mex

Coplanar D-π-A organic sensitizers featuring a thienylethynyl spacer for efficient dye-sensitized solar cells

Kwang-Won Park[1], Sungwoo Ahn[1], Myung Hoon Baek[1], Dong-Suk Lim[1], Alan A. Wiles[2], Myung Gil Kim[1,*], and Jongin Hong[1,*]

[1] *Department of Chemistry, Chung-Ang University, Seoul 156-756, Republic of Korea*
[2] *Glasgow Centre for Physical Organic Chemistry, WestCHEM, School of Chemistry, University of Glasgow, Glasgow, G12 8QQ, UK*

ABSTRACT

We simply synthesize coplanar metal-free organic sensitizers featuring a thienylethynyl spacer, **CSD-01** and **CSD-02**, from commercially available thiophene derivatives. The dye-sensitized solar cells (DSSCs) based on the **CSD-01** and **CSD-02** without any coadsorbate show the power conversion efficiencies (η) of 4.60% and 5.32%, respectively. The study in the dye-adsorption time suggests the increase in the organic DSSC performance with decreasing soaking time.

Keywords: Dye Sensitized Solar Cell, Metal-Free Organic Dye, Theinylethynyl, Thiophene, Natural Bond Orbital.

1. INTRODUCTION

To address the depletion of finite fossil fuels and the global warming together with an everlasting global demand for energy, we have been searching for clean, renewable and cheap energy. Among naturally abundant energy resources, solar light radiates a huge amount of energy that would contribute to our electrical and chemical needs, a power level of 1,000 W/m^2. Accordingly, it is an undeniable fact that photovoltaic (PV) devices (or solar cells) have been extensively developed to meet the energy demand. Of particular note has been the considerable progress in the dye-sensitized solar cells (DSSCs) because of their distinctive features including flexibility in shape, color and transparency, and good performance under low light conditions and different solar incident angles.[1,2] Over the last few decades, many researchers have devoted their efforts to design and synthesize new photosensitizers, such as ruthenium polypyridine complexes and metal-free organic dyes.[3–7] Even if the ruthenium(II)-polypyridyl complexes allow for high power-conversion efficiency in DSSCs, these photosensitizers have major drawbacks, such as limited extinction coefficients, costly ruthenium metal and tricky purification.

In contrast, metal-free organic dyes offer several advantages including abundant raw materials, rich synthetic protocols and lower cost large-scale production. Among these organic dyes, the push-pull architecture, such as a dipolar D-π-A structure (i.e., donor (D) and acceptor (A) groups separated by a π-conjugated bridge), has been mostly adopted. The dyes can be easily tuned up by structural modification with the incorporation of substituents into chromophore skeletons.[7–9] For example, triphenylamine derivatives are commonly selected as the electron donor (D). A cyanoacrylic acid moiety is used as the electron acceptor (A) and anchoring unit for electron injection into TiO_2. Various π-conjugation bridges, such as benzene, furan and thiophene, have been

*Authors to whom correspondence should be addressed.
Emails: myunggil@cau.ac.kr, hongj@cau.ac.kr

Article

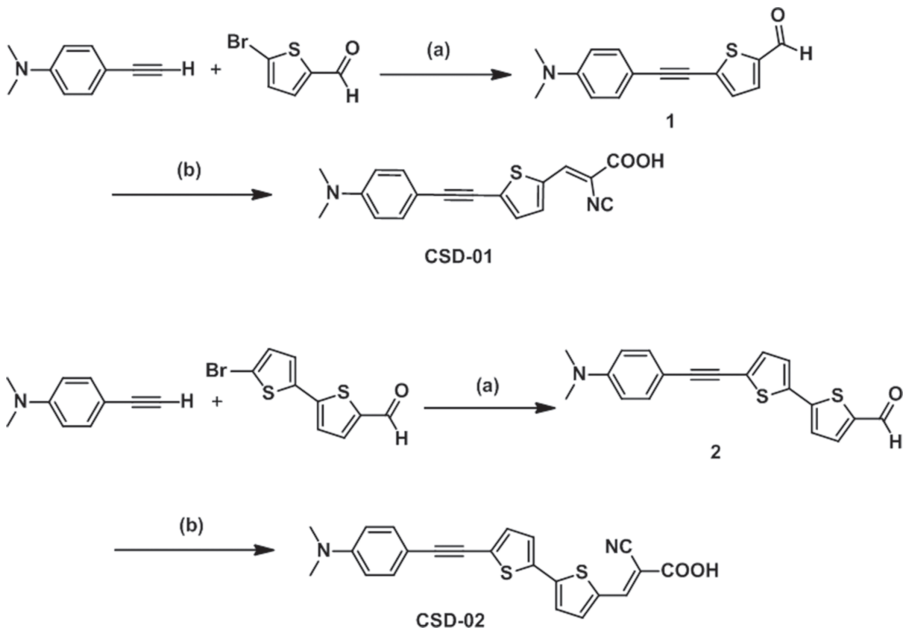

Fig. 1. Reagents and conditions: (a) $Pd(PPh_3)_2Cl_2$, CuI, PPh_3, triethylamine (TEA); (b) cyanoacetic acid, piperidine, MeCN.

considered to extending the absorption spectra of the organic sensitizers.[10–12] The π-linker is of significant importance in modulating photophysical properties and its planarity should be considered to increase electron delocalization.[13, 14] In this study, we report a revised, improved, synthetic protocol of two metal-free organic compounds featuring a thienylethynyl spacer (Fig. 1) and their optical and electrochemical properties comparing with in depth theoretical calculations.[15] We also demonstrate the influence of soaking time and co-adsorbate over the performance of the DSSCs.

2. EXPERIMENTAL DETAILS

2.1. Materials

All chemicals including 5-bromo-2-carboxaldehyde, 5-bromo-2,2′-bithiophene-5′-carboxaldehyde and 4-ethynyl-*N*,*N*-dimethylaniline were purchased from Sigma Aldrich or TCI and then used without further purification. All solvents were dried and distilled. All reactions were undertaken under either dry nitrogen or argon atmosphere.

2.2. Characterization

NMR spectroscopy was undertaken on a Bruker AVIII (400 MHz) spectrometer. Chemical shifts are reported in ppm and are relative to tetramethylsilane (TMS). Element analyses were performed by investigation of C, H, N, O and S. Melting point and degradation temperatures were determined with DSC and TGA under argon atmosphere. UV-VIS spectra were recorded on a JASCO UV/Vis/NIR spectrophotometer. Optical band gaps (E_g) were estimated using the absorption edge of the longest wavelength absorption (λ) using $E_g = 1240/\lambda$. An attenuated total reflection (ATR)-FTIR spectrometer (Vertex 80, Bruker Optics, Germany) with an image microscope (Hyperion 3000, Bruker Optics, Germany) was used to determine *E* and *Z* configurations of 2-cyano-3-(thiophen-2-yl)acrylic acid (TCA). Square wave voltammetry (SWV) was conducted using a CH Instruments 440a electrochemical analyzer using a platinum disc working electrode, a platinum wire counter electrode and a silver wire pseudo-reference electrode. Ferrocene was used as an external standard and all redox couples are reported versus ferrocene/ferrocenium ($Fc/Fc^+ = -4.8$ eV) redox couple (adjusted to 0.0 V). The solutions were prepared using dry dimethylformamide (DMF) containing 0.1 M of tetrabutylammonium hexafluorophosphate ($TBAPF_6$) as a supporting electrolyte. The solutions were purged with nitrogen gas for 3 min prior to recording the electrochemical data. Dye desorption was accomplished by immersing the dye-sensitized TiO_2 films into 0.1 M NaOH in deionized water:ethanol:THF (1:1:1) and then the dye adsorption was determined as a function of soaking time.

2.3. Computational Details

Density functional theory (DFT) and time-dependent density functional theory (TDDFT) calculations were performed using Gaussian '09 package.[16] All geometries were optimized using Becke's three-parameter hybrid and Lee-Yang-Parr's gradient corrected correlation (B3LYP) functional and 6-311G (d, p) basis set without additional diffused function. None of the vibrational frequencies in the optimized geometries generated negative frequencies in their ground state. Natural bond orbital (NBO) analysis were conducted by calculating the orbital populations with the B3LYP/6-311G (d, p) method at

Article

the ground state. TDDFT calculations were performed on the basis of the ground-state optimized geometries with Coulomb-attenuating B3LYP (CAM-B3LYP) functional under 6-311++G (d, p) basis set level of theory in acetonitrile ($\varepsilon = 35.688$) environment by means of the Tomasi's polarized continuum model (PCM).

2.4. Syntheses

To synthesize 5-(2-(4-(*N*,*N*-dimethylamino)phenyl)ethynyl) thiophene-2-carbaldehyde (**4**), $Pd(PPh_3)_2Cl_2$ (0.24 g, 0.344 mmol), PPh_3 (0.036 g, 0.138 mmol), CuI (0.013 g, 0.069 mmol) and 4-ethynyl-*N*,*N*-dimethylaniline (1.0 g, 6.89 mmol) were added to a solution of 5-bromo-2-carboxaldehyde (1.32 g, 6.89 mmol) in TEA (30 mL) under nitrogen. The mixture was stirred at reflux for 3 h under nitrogen. The mixture was cooled to room temperature and water (50 mL) was added. The reaction mixture was extracted with dichloromethane (DCM) (2×50 mL) and the combined organic layers were washed with HCl (2 N; 2×50 mL) and brine (50 mL), dried over $MgSO_4$, filtered and evaporated *in vacuo*. The crude product was purified by silica gel column chromatography (2:1 MC:Hexane) to give a yellow solid (1.6 g, 91%). ^{1}H NMR (400 MHz, $CDCl_3$) δ 9.84 (s, 1H), 7.64 (d, $J = 3.9$ Hz, 1H), 7.41 (d, $J = 8.9$ Hz, 2H), 7.22 (d, $J = 3.9$ Hz, 1H), 6.65 (d, $J = 8.9$ Hz, 2H), 3.02 (s, 6H) ppm; ^{13}C NMR (100 MHz, $CDCl_3$) δ 182.3, 150.7, 142.7, 136.4, 134.6, 133.0, 131.4, 111.6, 108.1, 100.4, 80.6, 40.1 ppm; MS m/z(EI+) calculated for $C_{15}H_{13}NOS$ 255.1 found 255.1.

To synthesize (E)-3-(5-(4-(*N*,*N*-dimethylamino)phenyl) ethynyl)thiophene-2-yl)-2-cyanoacrylic acid (**CSD-01**), 2-cyanoacetic acid (0.99 g, 11.59 mmol) and piperidine (1.48 g, 17.39 mmol) were added to a solution of compound 4 (1.48 g, 5.78 mmol) in MeCN (50 mL). The mixture was stirred at reflux for 3 h. The mixture was cooled to room temperature and water (100 mL) was added. The reaction mixture was extracted with DCM (2×100 mL) and the combined organic layers were washed with HCl (2 N; 2×50 mL) and brine (50 mL), dried over $MgSO_4$, filtered and evaporated *in vacuo*. The crude product was dissolved in methanol and washed with hexane, the solvent was removed *in vacuo* to give pure CSD-01 as a dark grey powder (0.99 g, 53%). Melting point: 238.72 °C. ^{1}H NMR (400 MHz, DMSO) δ 8.50 (s, 1H), 7.97 (d, $J = 4.3$, 1H), 7.47 (d, $J = 4.0$, 1H), 7.43 (d, $J = 9.0$, 2H), 6.75 (d, $J = 9.1$, 2H) 2.99 (s, 6H) ppm; ^{13}C NMR (100 MHz, DMSO) δ 163.4, 150.8, 146.0, 140.3, 135.4, 132.8, 132.1, 131.8, 116.5, 111.8, 106.6, 101.3, 80.8, 39.6 ppm; FT-IR (ATR) υ 2913, 2807, 2172, 1678, 1599 cm^{-1} MS m/z(EI+) calculated for $C_{18}H_{14}N_2O_2S$ 322.1 found 322.1. Anal. Calcd for $C_{18}H_{14}N_2O_2S$: C, 66.36; H, 441; N, 8.77; O, 9.79; S, 9.85.

To synthesize 5-(5-(2-(4-(*N*,*N*-dimethylamino)phenyl) ethynyl)thiophene-2-yl)thiophene-2-carbaldehyde (**5**), $Pd(PPh_3)_2Cl_2$ (0.24 g, 0.342 mmol), PPh_3 (0.036 g, 0.136 mmol), CuI (0.026 g, 0.136 mmol) and 4-ethynyl-*N*,*N*-dimethylaniline (1.04 g, 7.14 mmol) were added to a solution of 5-Bromo-2,2′-bithiophene-5′-carboxaldehyde (1.86 g, 6.80 mmol) in TEA (60 mL) under nitrogen. The mixture was stirred at reflux for 4 h under nitrogen. The mixture was cooled to room temperature and water (100 mL) was added. The reaction mixture was extracted with DCM (2×100 mL) and the combined organic layers were washed with HCl (2 N; 2×100 mL) and brine (100 mL), dried over $MgSO_4$, filtered and evaporated *in vacuo*. The crude product was purified by silica gel column chromatography (2:1 MC:Hexane) to give a brown solid (1.59 g, 69%). ^{1}H NMR (400 MHz, $CDCl_3$) δ 9.86 (s, 1H), 7.67 (d, $J = 4.0$, 1H), 7.39 (d, $J = 8.3$, 2H), 7.23 (d, $J = 3.4$, 1H), 7.22 (d, $J = 3.4$, 1H), 7.13 (d, $J = 3.9$, 1H), 6.66 (d, $J = 8.8$, 2H), 3.01 (s, 6H) ppm; ^{13}C NMR (100 MHz, $CDCl_3$) δ 182.4, 150.4, 146.6, 141.6, 137.3, 135.8, 132.7, 131.8, 126.3, 126.0, 124.2, 111.7, 108.8, 97.3, 80.2, 40.1 ppm; MS m/z(EI+) calculated for $C_{19}H_{15}NOS_2$ 337.3 found 337.1.

To synthesize (E)-3-(5-(5-(2-(4-(*N*,*N*-dimethylamino) phenyl)ethynyl)thiophene-2-yl)thiophene-2-yl)-2-cyanoacrylic acid (**CSD-02**), 2-cyanoacetic acid (0.80 g, 9.42 mmol) and piperidine (1.20 g, 14.12 mmol) were added to a solution of compound **5** (1.59 g, 4.71 mmol) in DCM (20 mL), MeCN (20 mL), toluene (60 mL). The mixture was stirred at reflux for overnight. The mixture was cooled to room temperature and water (50 mL) was added. The reaction mixture was extracted with DCM (2×200 mL) and the combined organic layers were washed with HCl (2 N; 2×100 mL) and brine (100 mL), dried over $MgSO_4$ filtered and evaporated *in vacuo*. The crude product was dissolved in methanol and washed with hexane, the solvent was removed *in vacuo* to give pure CSD-02 as a dark grey powder (1.06 g, 56%). Melting point: 243.70 °C. ^{1}H NMR (400 MHz, DMSO) δ 8.47 (s, H), 7.97 (d, $J = 4.2$, 1H), 7.60 (d, $J = 4.0$, 1H), 7.56 (d, $J = 3.9$, 1H), 7.37 (d, $J = 9.0$, 2H), 7.33 (d, $J = 3.9$, 1H), 6.72 (d, $J = 9.1$, 2H), 2.97 (s, 6H) ppm; ^{13}C NMR (100 MHz, DMSO) δ 164.3, 151.3, 146.9, 145.3, 142.0, 136.2, 135.3, 134.2, 133.7, 133.3, 128.1, 126.4, 125.7, 117.4, 112.7, 108.0, 98.6, 81.1, 40.5 ppm; IR (film) υ 2921, 2852, 2182, 1673, 1603 cm^{-1}; MS m/z(EI+) calculated for $C_{22}H_{16}N_2O_2S_2$ 404.2 found 404.1. Anal. Calcd for $C_{22}H_{16}N_2O_2S_2$: C, 63.52, H, 4.29; N, 6.50; O 8.52; S, 14.50.

2.5. DSSC Fabrication and Photovoltaic Measurements

The inverse micelles containing ytterbium (III) chloride were spin-coated onto transparent fluorione-doped SnO_2 (FTO)-coated conducting glass (TEC 8, Pilkington, Sheet resistance = 8Ω/□) at 2000 rpm for 60 s. The zero-dimensional ytterbium oxide nanodots on the substrate

were formed after eliminating the polymer template by O_2 plasma etching. More details about their preparation can be found in Ref. [17]. 20 nm-TiO_2 photoanodes were screen-printed on the ytterbium oxide nanodot arrays and the resulting layers were sintered at 525 °C for 3 hours in a muffle furnace. Subsequently, 500 nm-TiO_2 scattering layers were screen-printed on the photoanodes and then thermally sintered at 525 °C for 3 hours in a muffle furnace. Active areas of the electrodes were 0.20 cm^2. The prepared TiO_2 electrodes were immersed in a 0.04 M $TiCl_4$ solution at 75 °C for 30 min. They were rinsed with deionized water and ethanol and then sintered at 500 °C for 30 min on a hot plate. The electrodes were exposed to O_2 plasma for 10 min and then immersed into a 0.5 mM photosensitizer (N719, **CSD-01** and **CSD-02**) solution in ethanol for various hours. A co-adsorbate such chenodeoxycholic acid (CDCA) was also introduced into the dye solution. Pt counter electrodes were prepared by thermal reduction of 20 mM chloroplatinic acid (H_2PtCl_6, Sigma-Aldrich) in 2-propanol at 525 °C for 1 hr in a muffle furnace. Both the photosensitizer-anchored photoanode and the platinzed counter electrode were assembled using a 25 μm-thick thermoplastic Surlyn (Solaronix). A commercially available iodide electrolyte (AN-50, Solaronix) was filled through the pre-drilled holes in the counter electrode.

The photovoltaic characteristics of the devices were measured by using a solar cell I–V measurement system (K3000 LAB, McScience, Korea) under both AM1.5 global one sun illumination (100 mW/cm^2) and dark conditions. Short-circuit photocurrent density (J_{sc}), open-circuit voltage (V_{oc}), fill factor (FF) and power conversion efficiency (η) were measured simultaneously. Monochromatic incident photon-to-current conversion efficiency (IPCE) was recorded to evaluate the spectral response of solar cells (QEX7, PV Measurements, USA). Electrochemical impedance spectroscopy (EIS) measurements were performed with DSSCs biased to V_{oc} under illumination and in dark by using a frequency response analyzer (Solartron 1260). A sinusoidal potential perturbation with an amplitude of 100 mV was applied over a frequency range of 0.1 Hz to 100 kHz.

3. RESULTS AND DISCUSSION

3.1. Characterization

The two compounds, **CSD-01** and **CSD-02**, were synthesized in a simple two-step protocol (Fig. 1). Sonogashira coupling reactions of compound **1** or **2** with **3** provided compounds **4** and **5** respectively, which were further condensed with cyanoacetic acid under Knoevenagel condensation conditions to obtain **CSD-01** or **CSD-02**. Figure 2(a) shows the UV-visible absorption spectra of the compounds in DMF solution and dye-grafted mesoporous TiO_2 films. The distinct absorption band in the visible region is attributed to the intramolecular charge transfer (ICT) between the D and A moieties. The addition of another thiophene unit resulted in redshift in the maximum absorption wavelength, presumably a consequence of extending the conjugation. The molar extinction coefficients of **CSD-01** and **CSD-02** in DMF were 52,900 M^{-1} cm^{-1} and 70,400 M^{-1} cm^{-1}, respectively. The optically determined band gaps were 2.52 eV and 2.41 eV for **CSD-01** and **CSD-02**, respectively. Compared with the spectra in DMF solution, the ICT absorption band of the two dyes on TiO_2 films exhibits significant spectral broadening and bathochromic shift because of the interaction of the anchoring groups with the surface of TiO_2 and J-aggregation of photosensitizer molecules (Fig. 2(b)). Emission spectra of the two dyes are shown in Figure 2(c). CSD-01 and CSD-02 feature the emission maximum at 563 nm and 572 nm, respectively. The shift of the photoluminescence maximum to longer wavelengths is due to the extension of the π-conjugation. No emission from the dye-adsorbed TiO_2 films was observed. The electrochemical behavior of the two compounds was explored by SWV (Fig. 2(d)). The reversible oxidation potentials of the dyes originate from the phenylamine unit are measured as +0.47 V and +0.49 V versus Fc/Fc^+ for **CSD-01** and **CSD-02**, respectively. On the contrary, the reduction wave potentials are shifted from −2.08 V for **CSD-01** to −1.88 V for **CSD-02** indicating that the additional thiophene unit is easier to reduce. According to the energy level of Fc/Fc^+ redox couple (4.8 eV under vacuum level[18]), the highest occupied molecular orbital (HOMO) and the lowest unoccupied molecular orbital (LUMO) levels are estimated as listed in Table I. The LUMO value of **CSD-02** is lower than that of **CSD-01**, resulting in a lower band gap for **CSD-02** (2.39 eV) compared to **CSD-01** (2.57 eV). The electrochemically determined band gaps are in reasonable accordance with those determined optically.

3.2. Theoretical Calculations

Figure 3(a) shows the optimized geometries of the **CSD-01** and **CSD-02** photosensitizers. Coplanar molecular structures indicate that the organic dyes are fully conjugated throughout the donor, π-bridge and acceptor groups. The acetylene and thiophene linker groups allow for maintaining such planar structures, which can suppress rotational disorder and enhance electron transfer. At the HOMO level, the electron is uniformly delocalized from the donor to the π-bridge for both dyes, indicating a feature for an efficient electron transfer. In contrast, at the LUMO level, the excited electron is extended over the π-conjugation and acceptor groups and thus this is beneficial to the electron injection into TiO_2 via the cyanoacrylic acid unit. **CSD-02** exhibits more localized electron density distribution than CSD-01. From the molecular orbital (MO) energy levels of the two dyes in Figure 3(b), the increase in the π-conjugation results in the smaller HOMO

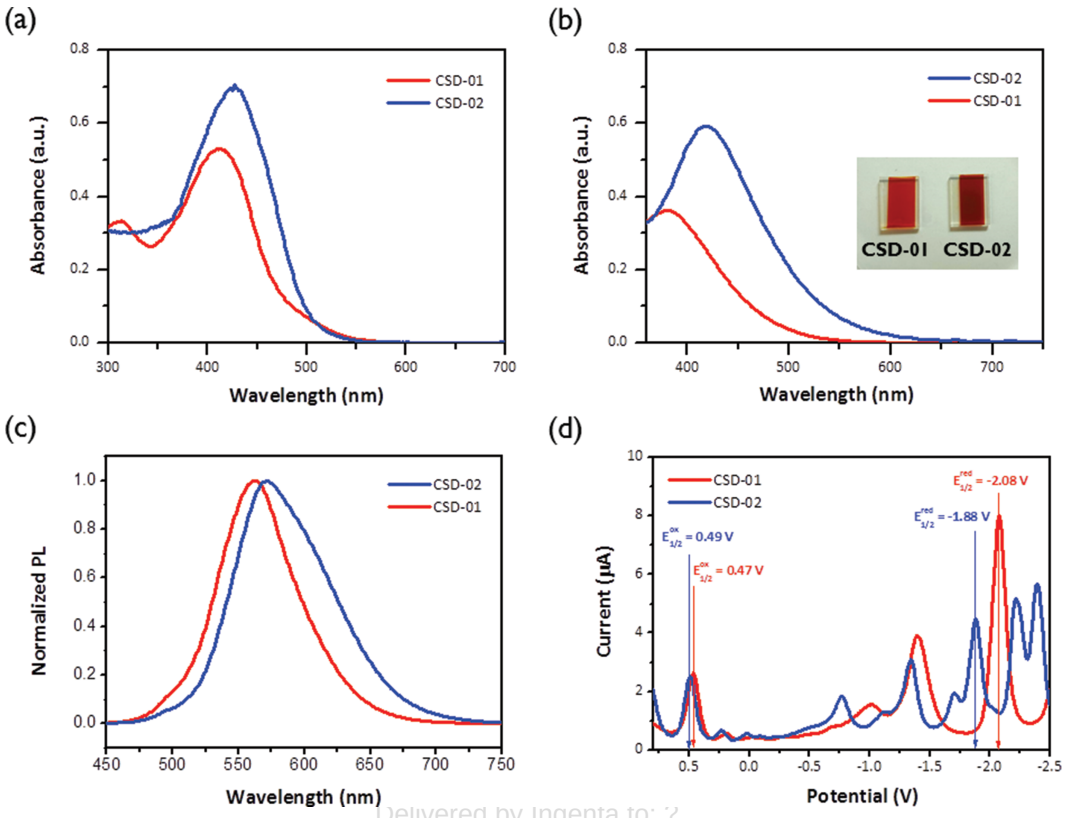

Fig. 2. (a) UV-Vis absorption spectra of the organic dyes in DMF solution (1×10^{-5} M) and (b) on TiO_2 films, (c) photoluminescence spectra and (d) square wave voltammetry of the dyes recorded in DMF solution.

and LUMO band gaps and consequently red-shifting the absorption.

Recently, we reported that bond lengths in the metal-free organic D-π-A dyes would have a strong correlation with their charge transfer and optical properties.[19] The selected bond lengths (denoted as d_1, d_2, d_3, d_4 and d_5) are summarized in Table II. The addition of the second thiophene unit results in the increase in d_1, d_2 and d_3 but the decrease in d_4 and d_5. This trend may be used as a relative descriptor for how much the intramolecular charge transfer (ICT) between the D and A moieties is enhanced. In order to quantitatively characterize the direction and amount of the charge separation between the D and A moieties, second order perturbation theory (SOPT) analysis within the natural bond orbital (NBO) basis was performed. Conjugative interaction energies (ΔE) between the π and π^* orbitals in **CSD-01** and **CSD-02** are summarized in Table III. The conjugative interaction energy from C5═C6 to C7═C8 of **CSD-02** is higher than that of **CSD-01**. This implies that longer conjugation length would facilitate more charge transfer from the donor to acceptor.

In addition, *E* and *Z* configuration of 2-cyano-3-(thiophene-2-yl)acrylic acid (TCA) of both **CSD-01** and **CSD-02** can be obtained during synthesis and thus we performed the ground-state potential energy surface scan of the *E* and *Z* configuration as a function of the dihedral angle between the thiophene and cyanoacrylic acid. The calculated energy difference between *E* and *Z* conformers of **CSD-01** and **CSD-02** is 12.58 kJ/mol and 12.82 kJ/mol, respectively. As reported to similar molecules, the *E* configuration (thiophene and CN are in *cis* configuration) is more energetically stable than the *Z* configuration (thiophene and COOH are in *cis* configuration).[20] We think that this would be related to the steric hindrance between thiophene and cyanoacrylic acid moieties. Considering the significant rotational energy barrier (190~270 kJ/mol) along the double bond, the stable *E* geometry of the molecules could be retained during the dye adsorption on the TiO_2 surface.[21]

Table I. Redox properties of CSD-01 and CSD-02.

	$E_{1/2}$ (ox) (V)	$E_{1/2}$ (red) (V)	E_{HOMO} (eV)	E_{LUMO} (eV)	E_g (E chem) (eV)
CSD-01	0.47	−2.08	−5.27	−2.72	2.55
CSD-02	0.49	−1.88	−5.29	−2.92	2.37

3.3. Photovoltaic Performance

The photovoltaic properties of the fabricated DSSCs with increasing soaking time were measured under 1 sun (AM 1.5G) simulated light and summarized in Table IV.

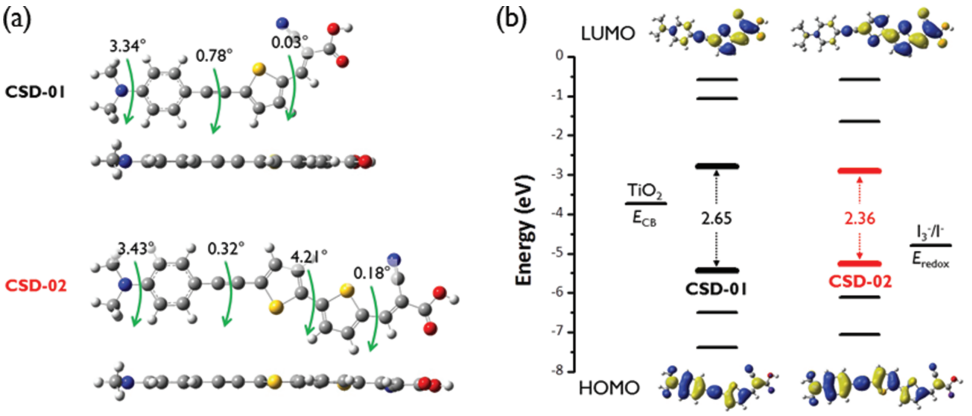

Fig. 3. (a) Optimized structures, (b) calculated frontier molecular orbitals and energy levels of **CSD-01** and **CSD-02**.

Table II. Selected bond length values of **CSD-01** and **CSD-02** dyes obtained by using B3LYP/6-311G(*d*, *p*) method in gas phase.

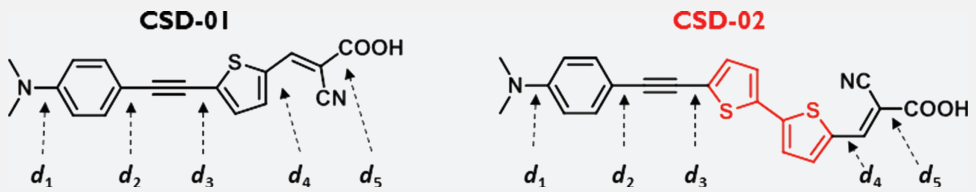

	Selected bond lengths (Å)				
Dyes	d_1	d_2	d_3	d_4	d_5
CSD-01	1.37477	1.41225	1.39615	1.42013	1.48482
CSD-02	1.37620	1.41427	1.39771	1.41905	1.48468

As the soaking time increased, the dye adsorption on TiO_2 surface increased. Unfortunately, both J_{sc} and V_{oc} values decrease continuously with increasing dye adsorption time. Because of the aggregation of dye molecules on the TiO_2 surface, prolonged dye-soaking time allows for lowering DSSC performance. The trend in J_{sc} and V_{oc} can be attributed to the increase in π–π stacking interaction between molecules and electron–hole recombination from the conduction band of the TiO_2 film to the I_3^- in the electrolyte, respectively. The addition of dye aggregation suppresser, CDCA, to the soaking solution resulted in the increase in V_{oc} and fill factor (FF) and the decrease in J_{sc}. Figure 4(a) shows J–V characteristics of DSSCs sensitized with **CSD-01** and **CSD-02** of 1 hr adsorption with or without CDCA. Although open circuit voltage (V_{oc}) values of the two dyes are almost the same, the addition of the second thiophene linker unit resulted in better photovoltaic performance: J_{sc} from 11.44 mA/cm^2 to

Table III. Conjugative interaction energies (ΔE, in kcal/mol) between the π and π^* orbitals in organic dyes (**CSD-01** and **CSD-02**) from the SOPT analysis within NBO calculation.

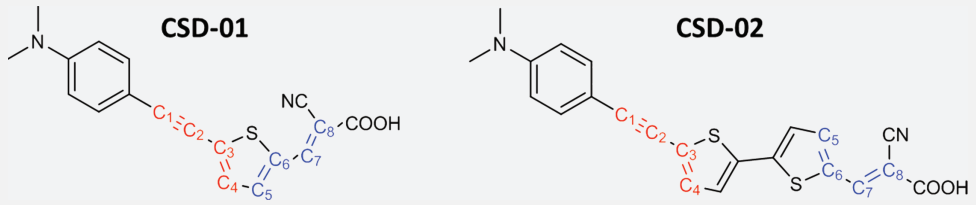

Dyes	Donor orbital (π)	Acceptor orbital (π^*)	ΔE	$E_{acc} - E_{don}$/a.u.	F (acc,don)/a.u.
CSD-01	π (C1≡C2)	π^* (C3═C4)	15.82	0.29	0.064
	π (C5═C6)	π^* (C7═C8)	26.11	0.30	0.079
CSD-02	π (C1≡C2)	π^* (C3═C4)	14.94	0.29	0.063
	π (C5═C6)	π^* (C7═C8)	26.25	0.30	0.080

Article

Table IV. Photovoltaic performance of DSSCs based on **CSD-01** and **CSD-02** as a function of dye-soaking time.

Dyes	Soaking time (hr)	Dye adsorption (nmol/cm^2)	V_{oc} (V)	J_{sc} (mA/cm^2)	FF	η(%)
CSD-01	1	0.167	0.57	11.44	70.3	4.60
	1 (CDCA)	0.155	0.58	10.90	72.1	4.59
	3	0.177	0.57	10.55	72.6	4.38
	6	0.182	0.56	9.99	68.7	3.81
	12	0.194	0.54	9.72	71.5	3.78
	18	0.203	0.53	9.06	71.2	3.42
CSD-02	1	0.138	0.58	13.71	67.3	5.32
	1 (CDCA)	0.130	0.59	13.40	70.4	5.58
	3	0.148	0.57	13.17	69.4	5.25
	6	0.162	0.54	12.09	69.8	4.60
	12	0.202	0.53	11.86	69.6	4.40
	18	0.260	0.51	11.25	68.5	3.96

13.71 mA/cm^2 and power-conversion-efficiency (η) from 4.60% to 5.32%. Importantly, CDCA suppresses the dark current. Dark current in DSSC mainly results from the loss of the injected electron from TiO_2 to I_3^- and thus the reduced dark current improved the open-circuit voltage of the DSSC. Figure 4(b) shows IPCE spectra for the DSSCs according to the following equation:

$$\text{IPCE} = \frac{1240\ (\text{eV}\cdot\text{nm})\cdot J_{sc}\ (\text{mA}\cdot\text{cm}^{-2})}{\lambda\ (\text{nm})\cdot\varphi\ (\text{mW}\cdot\text{cm}^{-2})}$$

where J_{sc} is the short-circuit photocurrent density for monochromatic irradiation, λ and φ are the wavelength and the intensity of the monochromatic light, respectively. The IPCE of **CSD-02** displays a broader band between 300 and 800 nm than that of **CSD-01**. The aforementioned results demonstrate that the addition of the second π-bridge between the D and A moieties broaden the visible absorption spectrum both in solution and upon deposition onto TiO_2. We think that this could be responsible for the significant enhancement of DSSC performance (4.60% of **CSD-01** to 5.32% of **CSD-02**). Figure 4(c) shows the Nyquist plots to study the interfacial charge transfer processes of DSSCs in dark. The first semicircle in the high frequency region is assigned to the redox reaction of I^-/I_3^- at the counter electrode/electrolyte interface. The second semicircle in the intermediate frequency region reflects the charge recombination between electrons in the TiO_2 photoanode with I_3^- ions in the electrolyte. The radius of the second semicircle is directly related to the charge recombination resistance (i.e., a larger radius indicates a slower charge recombination). The recombination resistance decreases in the order of **CSD-01** > **CSD-02**. This confirms lower dark current of **CSD-01** than **CSD-02**. Under illumination with applied open-circuit voltage (Fig. 4(d)), the intermediate frequency semicircle reflects charge-transfer resistance at the TiO_2/dye/electrolyte interface and its radius decreases

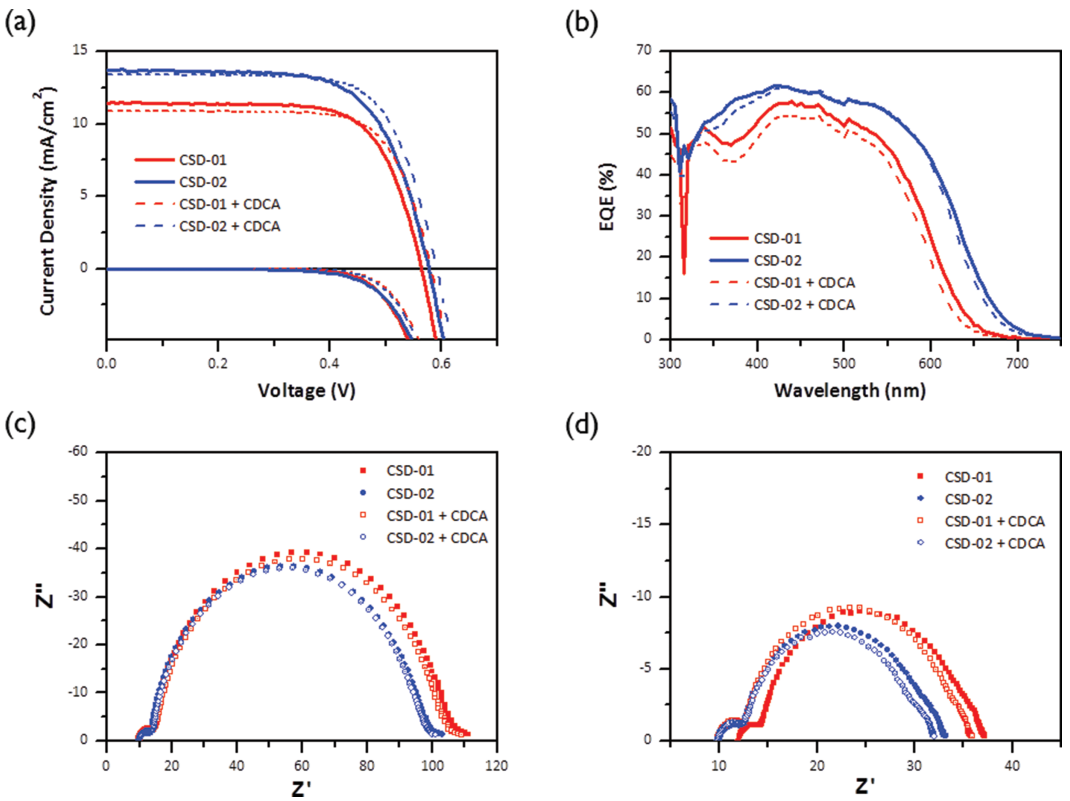

Fig. 4. (a) J–V characteristics, (b) IPCE spectra ad Nyquist plots (c) in dark and (d) under illumination of the DSSCs sensitized with **CSD-01** and **CSD-02** dyes for 1 hr.

in the order of **CSD-01** > **CSD-02**. This implies that **CSD-02** has higher electron transport than **CSD-01**. This trend coincides with higher photocurrent of **CSD-02** than **CSD-01**.

4. CONCLUSION

In summary, we improved on the synthesis of coplanar metal-free organic dyes **CSD-01** and **CSD-02**. The D-π-A structure, featuring a thienylethynyl spacer, from commercially available materials allows for cheap and easy access to these sensitizers. The additional thiophene bridging unit in **CSD-02**, allowing for enhanced light-harvesting ability compared to **CSD-01**, resulted in better photovoltaic performance: η from 4.60% to 5.32%. Interestingly, study in the dye-adsorption time resulted in the decrease in the organic DSSC performance with increasing soaking time. We hope that this paper will encourage such coplanar metal-free organic dyes to be used for further development in lower cost photovoltaic applications.

Acknowledgments: This research was supported by the Chung-Ang University Research Scholarship Grants in 2014 and the international Cooperative R&D program through Korea Institute for Advancement of Technology (KIAT) funded by the Ministry of Trade, Industry and Energy (MOTIE) of Korea.

References and Notes

1. S. Zhang, X. Yang, Y. Numata, and L. Han; Highly efficient dye-sensitized solar cells: Progress and future challenges; *Energ. Environ. Sci.* 6, 1443 (**2013**).
2. A. Fakharuddin, R. Jose, T. M. Brown, F. Fabregat-Santiago, and J. Bisquert; A perspective on the production of dye-sensitized solar modules; *Energ. Environ. Sci.* 7, 3952 (**2014**).
3. J. N. Clifford, E. Martinez-Ferrero, A. Viterisi, and E. Palomares; Sensitizer molecular structure-device efficiency relationship in dye sensitized solar cells; *Chem. Soc. Rev.* 40, 1635 (**2011**).
4. Md. K. Nazeeruddin, S. M. Zakeeruddin, J.-J. Lagref, P. Liska, P. Comte, C. Barolo, G. Viscardi, K. Schenk, and M. Graetzel; Stepwise assembly of amphiphilic ruthenium sensitizers and their applications in dye-sensitized solar cell; *Coord. Chem. Rev.* 248, 1317 (**2004**).
5. A. Hagfeldt, G. Boschloo, L. Sun, L. Kloo, and H. Pettersson; Dye-sensitized solar cells; *Chem. Rev.* 110, 6595 (**2010**).
6. A. Mishra, M. K. R. Fischer, and P. Bäerle; Metal-free organic dyes for dye-sensitized solar cells: From structure: Property relationships to design rules; *Angew. Chem. Int. Ed.* 48, 2474 (**2009**).
7. R. K. Kanaparthi, J. Kandhadi, and L. Giribabu; Metla-free organic dyes for dye-sensitized solar cells: Recent advances; *Tetrahedron* 68, 8383 (**2012**).
8. M. Liang and J. Chen; Arylamine organic dyes for dye-sensitized solar cells; *Chem. Soc. Rev.* 42, 3453 (**2013**).
9. A. Mahmood, Triphenylamine based dyes for dye sensitized solar cells: A review; *Solar Energy* 123, 127 (**2016**).
10. R. Li, X. Lv, D. Shi, D. Zhou, Y. Cheng, G. Zhang, and P. Wang; Dye-sensitized solar cells based on organic sensitizers with different conjugated linkers: Furan, bifuran, thiophene, bithiophene, selenophene, and biselenophene; *J. Phys. Chem. C* 113, 7469 (**2009**).
11. Y. Wu and W. Zhu; Organic sensitizers from D-π-A to D-A-π-A: Effect of the internal electron-withdrawing units on molecular absorption, energy levels and photovoltaic performances; *Chem. Soc. Rev.* 42, 2039 (**2013**).
12. P. Kumaresan, S. Vegiraju, Y. Ezhumalai, S. L. Yau, C. Kim, W.-H. Lee, and M.-C. Chen; Fused-thiophene based materials for organic photovoltaics and dye-sensitized solar cells; *Polymers* 6, 2645 (**2014**).
13. Z.-S. Huang, X.-F. Zang, T. Hua, L. Wang, H. Meier, and D. Cao; 2,3-dipentyldithieno[3,2-f:2′,3′-h]quinoxaline-based organic dyes for efficient dye-sensitized solar cells: Effect of π-bridges and electron donors on solar cell performance; *ACS Appl. Mater. Interfaces* 7, 20418 (**2015**).
14. Z. Iqbal, W.-Q. Wu, Z.-S. Huang, L. Wang, D.-B. Kuang, H. Meier, and D. Cao; Trilateral π-conjugation extensions of phenothiazine-based dyes enhance the photovoltaic performance of the dye-sensitized solar cells; *Dyes Pigm.* 124, 63 (**2016**).
15. M. Al-Eid, S. Lim, K.-W. Park, B. Fitzpatrick, C.-H. Han, K. Kwak, J. Hong, and G. Cooke; Facile synthesis of metal-free organic dyes featuring a thienylethynyl spacer for dye sensitized solar cells; *Dyes Pigm.* 104, 197 (**2014**).
16. Gaussian, R. A., I, M. J. Frisch, G. W. Trucks, H. B. Schlegel, G. E. Scuseria, M. A. Robb, J. R. Cheeseman, G. Scalmani, V. Barone, B. Mennucci, G. A. Petersson, et al.; Gaussian Inc., Wallingford CT (**2009**).
17. K.-W. Park, S. Ahn, S.-H. Lim, M. H. Jin, J. Song, S.-Y. Yun, H. M. Kim, G. J. Kim, K. M. Ok, and J. Hong; Ytterbium oxide nanodots via block copolymer self-assembly and their efficacy to dye-sensitized solar cells; *Appl. Surf. Sci.* 364, 573 (**2016**).
18. J. Pommerehne, H. Vestweber, W. Guss, R. F. Mahrt, H. Bässler, M. Porsch, and J. Daub; Efficient two layer leds on a polymer blend basis; *Adv. Mater.* 7, 551 (**1995**).
19. D. Seo, K.-W. Park, J. Kim, J. Hong, and K. Kwak; DFT computational investigation of tuning the electron donating ability in metal-free organic dyes featuring a thienylethynyl spacer for dye sensitized solar cells; *Comput. Theor. Chem.* 1081, 30 (**2016**).
20. W. Zhu, Y. Wu, S. Wang, W. Li, X. Li, J. Chen, Z. Wang, and H. Tian; Organic D-A-π-A solar cell sensitizers with improved stability and spectral response; *Adv. Funct. Mater.* 21, 756 (**2011**).
21. V. Staemmler; CEPA calculations for rotational barriers about CC double bonds: Ethylene, allene, and methylene-cyclopropane; Energy Storage and Redistribution in Molecules; Plenum Press, New York (**1983**).

Received: 12 July 2016. Revised/Accepted: 29 November 2016.

Article